www.czasopisma.pan.pl PAN POLSKA AKADEMIA NAUK www.journals.pan.pl

A R C H I V E S O F M E T A L L U R G Y A N D M A T E R I A L S

Volume 58 2013 Issue 4

DOI: 10.2478/amm-2013-0157

J. WINCZEK*

THE ANALYSIS OF STRESS STATES IN STEEL RODS SURFACED BY WELDING

ANALIZA STANÓW NAPRĘŻENIA NAPAWANYCH PRĘTÓW STALOWYCH

In work is presented a method of calculating elasto-plastic states in thermally loaded rods, which takes into account phase transformations that occur during surfacing by welding. Kinetics of phase transformations during heating and cooling is limited by temperature values at the beginning and at the end of austenitic transformation, while the progress of phase transformations during cooling is determined on the basis of TTT-welding diagram, basing on Johnson-Mehl-Avrami-Kolomogorov law for diffusional transformations and Koistinen-Marburger for martensitic transformation. Stress state of a bar subjected to thermo-mechanical loads is described assuming the planar cross section hypothesis and using integral equations of stress equilibrium of a bar as well as simple Hook's law. Dependence of stresses from strains is assumed on the basis of tensile curves of particular structures, taking into account the influence of temperature. Computations of strains and stresses are investigated in a rod made of S235 steel, loaded by thermal fields generated by a point welding heat source of different intensities. The analysis of origination and development of plastic strains is carried out. In order to verify correctness of the model, experimental tests are carried out on a rod made of S235 steel surfaced with GMA method with geometry and welding parameters assumed in numerical simulations. Residual stresses, calculated taking into account phase transformations and for homogenous material model, are compared with experimental results.

Keywords: Phase transformation, Residual welding stresses, Stress measurement, Surfacing

W pracy przedstawiono sposób obliczeń stanów sprężysto – plastycznych w prętach obciążonych cieplnie, z uwzględnieniem przemian fazowych zachodzących podczas napawania. Kinetykę przemian fazowych podczas nagrzewania i chłodzenia limitują wartości temperatur początku i końca austenityzacji, natomiast postęp przemian podczas chłodzenia jest określony w oparciu o spawalniczy wykres ciągłego chłodzenia stali (CTP_C-S), bazując na prawach Johnsona-Mehla-Avramiego-Kołomogorova (JMAK) w odniesieniu do przemian dyfuzyjnych i Koistinena-Marburgera dla martenzytycznej. Stan naprężenia pręta poddanego działaniu obciążeń cieplno-mechanicznych opisano przyjmując hipotezę płaskich przekrojów oraz korzystając z całkowych równań równowagi pręta. Zależności naprężeń od odkształceń przyjęto na podstawie krzywych rozciągania poszczególnych struktur z uwzględnieniem wpływu temperatury. Wykonano obliczenia pola temperatury, przemian fazowych, odkształceń i naprężeń płaskownika wykonanego ze stali S235, obciążonego punktowym spawalniczym źródłem ciepła o różnej intensywności. Przeprowadzono analizę powstawania i rozwoju odkształceń plastycznych. W celu weryfikacji poprawności modelu przeprowadzono badania doświadczalne płaskownika wykonanego ze stali S235 napawanego metodą GMA, o geometrii i parametrach napawania przyjętych w symulacjach numerycznych. Porównano naprężenia własne obliczone z uwzględnieniem przemian fazowych oraz dla modelu materiału jednorodnego z wynikami badań doświadczalnych.

1. Introduction

Reasons for existence of residual stresses caused by the welding process of steel elements are well known. Two of them are temperature gradients and phase transformations, which in welding process cause plasticity. Along with temperature field and phase transformations indirect influence on plastic state has also change with temperature of thermo-mechanical properties, especially yield stress of welded material. This is because these properties change together with temperature and phase composition of steel.

Therefore, complete description of welding problems consists of changeable temperature field, phase transformations as well as stress and strain states connected by constitutive equation. Those fields interact with each other. Complete coupling of thermal, mechanical and material phenomena (phase changes) is often mentioned. Some of these couplings are in fact important for accurate calculations of welding problems, other have only research purposes.

In the Figure 1 has been presented the scheme of those couplings, where solid lines with marked arrows indicate relevant couplings, considered in this work, while dashed lines indicate couplings which have been omitted in this work as less important. Dotted line presents strain and stress state with temperature coupling, which in practice does not have significant meaning. Transformations caused by plastic strain of welding joints were discussed i.a. in works [1-11].

* CZĘSTOCHOWA UNIVERSITY OF TECHNOLOGY, INSTITUTE OF MECHANICS AND MACHINE DESIGN FOUNDATIONS, 73 DĄBROWSKI STR., 42-200 CZĘSTOCHOWA, POLAND

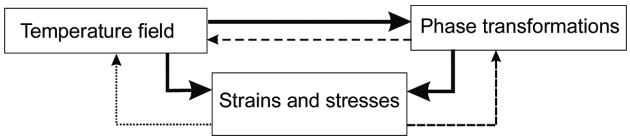

Fig. 1. Scheme of couplings

After welding, plastic strains and residual stresses have essential influence on the characteristics of welded steel product during its exploitation. In this range, scientific interests are concentrated on the following topics: simplified models, distribution of strains and stresses (especially in typical welded joints), the modelling states of stresses and strains in welding (taking into account phase transitions) and experimental analysis of detailed stress patterns (for the specified method of welding, types of connections and materials).

Intensive research into residual stresses was started in a half of the last century [12]. The simplified estimation methods of residual stress distribution for the typical welded joint were introduced, among others [13, 14].

A quantitative description of the changes in strains and stresses during welding is difficult and needs taking into account the complicated thermal processes and the dependence of thermo-mechanical properties on temperature [15]. Thus, the analysis of plasticity zones, formation and development of welding stresses, stays in the area of interest. Analytical methods are useful to analyse the formation and development of plastic strain and stress as well as to build the simplified schemes of residual stress distributions because they allow to evaluate quickly the stress field and influence of plasticity zones on the residual stresses.

2. Phase transforamations in solid state

Many works are devoted to the description and numerical modeling of steel phase transformations. The review of this kind of works is presented in [16]. The kinetics of phase transformation for diffusional transformations in the processes of heating and cooling are described by Johnson's and Mehl's, Avrami's and Kolomogorov's rules [17]. According to that, the amount of austenite η_A created during heating ferrite-pearlitic steel is defined according to the formula:

$$\eta_A = \sum_i \eta_i^0 \left(1 - \exp\left(-b_i t^{n_i}\right)\right) \tag{1}$$

where η_i^0 constitute initial fraction of ferrite ($i \equiv F$), pearlite ($i \equiv P$) and bainite ($i \equiv B$), while constants b_i and n_i are determined using conditions of beginning and end of the transformation.

In quantitative perspective the progress of phase transformation during cooling is estimated, using additivity rule, by voluminal fraction η_i of created phase what can be expressed analogically to Avrami's formula [18] – by equation [19]:

$$\eta_i = \eta_A \eta_i^{\max} \left(1 - \exp\left(-b_i t^{n_i}\right)\right) \tag{2}$$

where η_i^{max} is the maximum voluminal fraction of phase i (Fig. 2) while the integral voluminal fraction equals to:

$$\sum_{i=1}^{j} \eta_i = 1 \tag{3}$$

During regeneration surfaced areas first heat up and then cool down. As long as maximum temperature of heating exceeds temperature of initial austenitic transformation A_1 but does not exceed A_3, partial austenitic transformation occurs. If maximum temperature exceeds temperature A_3 original (initial) structure undergoes complete transformation in austenite. These transformations are described like for continuous process.

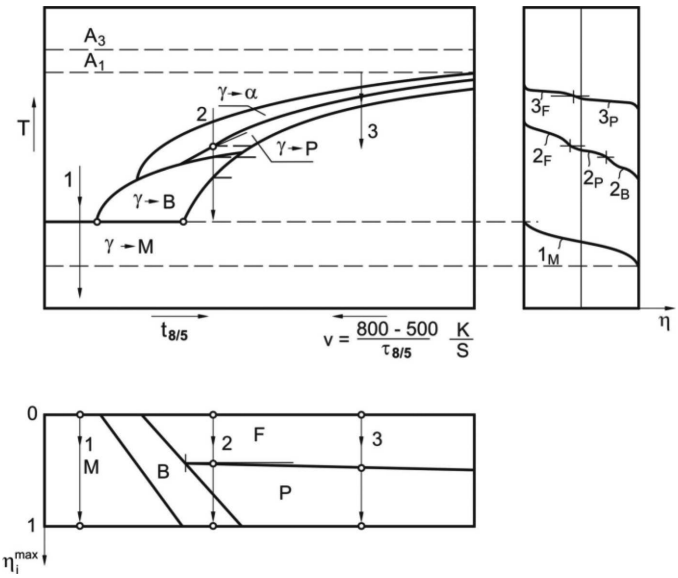

Fig. 2. Scheme of phase changes of overcooled austenite depending on cooling velocity within temperature range 800-500°C

In order to make quantitative description of dependence of structure and material quality on temperature and transformation time of austenite overcooled during surfacing, it is acceptable to use welding diagram time-temperature-transformation at continuous cooling (TTT-welding diagram). Description is made working on the assumption that cooling speed within 800-500°C temperature range is constant. These diagrams bind cooling $t_{8/5}$ (time of staying within temperature range between 500°C and 800°C) or speed of cooling ($v_{8/5}$ =$(800\text{-}500)/t_{8/5}$) and temperature with the progress of phase transformation (Fig. 2).

In quantitative perspective the progress of phase transformation is estimated by voluminal fraction η_i of created phase, where i could mean ferrite ($i \equiv F$), pearlite ($i \equiv P$), bainite ($i \equiv B$) or martensite ($i \equiv M$). Voluminal fraction η_i of created phase is expressed on the basis of formula (2), replacing time t with new independent variable which is temperature T [20]:

$$\eta_i = \eta_i^{\max} \left(1 - \exp\left(-b_i T^{n_i}\right)\right) \tag{4}$$

where:

$$n = \frac{\ln \dfrac{\ln\left(1 - \frac{\eta_i^f}{\eta_i^0}\right)}{\ln\left(1 - \frac{\eta_i^s}{\eta_i^0}\right)}}{\ln \dfrac{T_i^s}{T_i^f}} \tag{5}$$

$$b = \frac{\ln\left(1 - \dfrac{\eta_i^s}{\eta_i^0}\right)}{T_i^s} \tag{6}$$

$$\frac{\eta_i^s}{\eta_i^0} = 0.01 \tag{7}$$

$$\eta_i^f / \eta_i^{\max} = 0.99 \tag{8}$$

where $T_i^s = T_i^s(v_{8/5})$ and $T_i^f = T_i^f(v_{8/5})$ are respectively initial and final temperature of phase transformation i while η_i^0 denotes complete share of phase i in the whole blend.

The fraction of martensite formed below the temperature M_s is calculated using the Koistinen-Marburger formula [21-23]:

$$\eta_M = \eta_A \eta_M^{\max} \left(1 - \exp\left(-\mu \left(M_s - T\right)^m\right)\right), \tag{9}$$

$$\mu = -\frac{\ln\left(\eta_M^{\min} = 0.1\right)}{M_s - M_f}, \tag{10}$$

where: m is the constant, chosen by means of experiment; whereas μ is calculated basing on the condition that the transformation ends at temperature M_f.

3. Thermal and phase transformations strains

Total strain during single-pass surfacing represents the sum of thermal strains caused by phase transformation during heating and cooling:

$$\varepsilon^T(x, y, z, t) = \varepsilon^H + \varepsilon^C \tag{11}$$

where ε^H and ε^C – denote respectively thermal and phase transformation strains during heating and cooling.

Heating leads to the increased volume of material, while transformation of the initial structure (ferritic, pearlitic or bainitic) into austenite causes shrinkage connected with different densities of given structures. Then strains during heating are equal to:

$$\varepsilon^H = \varepsilon^{Th} - \varepsilon^{Trh} \tag{12}$$

where ε^{Th} is the strain caused by thermal expansion of the material:

$$\begin{aligned}\varepsilon^{Th} = \sum_{i=A,P,F,B,M} & \left(\alpha_i \eta_{i0} \left(T - T_0\right) H\left(T_{A_1} - T\right) + \right. \\ & + \alpha_i \eta_i \left(T - T_{A_1}\right) H\left(T_{A_3} - T\right) H\left(T - T_{A_1}\right) + \\ & \left. + \alpha_A \left(T - T_{A_3}\right) H\left(T - T_{A_3}\right)\right)\end{aligned} \tag{13}$$

while ε^{Trh} is the phase transformation strain during heating:

$$\varepsilon^{Trh} = \sum_{i=P,F,B,M} \eta_i \gamma_{iA} \tag{14}$$

where: γ_{iA} – structural strain of i-th structure in austenite, T_0 – initial temperature, α_i – linear thermal expansion coefficient of i-th structure, and $H(x)$ is the function defined as follows:

$$H(x) = \begin{cases} 1 & for\ x > 0 \\ 0.5 & for\ x = 0 \\ 0 & for\ x < 0 \end{cases} \tag{15}$$

Cooling of material causes its shrinkage, while transformation of austenite in cooling structures causes in turn the increase of its volume. It leads to complicated changes of strains dependent not only on current temperature of material during cooling but also on initial and final temperature of transformation of austenite into ferrite, pearlite, bainite or martensite as well as on voluminal shares of given structural constituents (including austenite). The strain during cooling can be determined basing on a relation:

$$\varepsilon^C = \varepsilon^{Tc} + \varepsilon^{Trc} \tag{16}$$

where ε^{Tc} is the strain caused by thermal shrinkage of material:

$$\begin{aligned}\varepsilon^{Tc} = & \alpha_A \left(T - T_{SOL}\right) H\left(T - T_s\right) + \\ & + \alpha_A \left(T_s - T_{SOL}\right) H\left(T_s - T\right) + \\ & + \sum_{i=A,P,F,B,M} \alpha_i \eta_i \left(T - T_{si}\right) H\left(T_{si} - T\right)\end{aligned} \tag{17}$$

while ε^{Trc} the strain caused by phase transformation during cooling,

$$\varepsilon^{Trc} = \sum_{i=P,F,B,M} \eta_i \gamma_{Ai} \tag{18}$$

where T_{SOL} is solidus temperature, T_s – initial temperature of phase transformation, T_{si} – initial temperature of austenite transformation in i-th structure, γ_{Ai} – structural strain of austenite in i-th structure. In addition, due to the limit on solid state of material:

$$\varepsilon^T = 0 \quad for \quad T > T_{SOL} \tag{19}$$

4. Stress states

4.1. Theoretical model

Temperature field $T = T(x_i, t)$ generates thermal strain αT. Temporary states of strains and stresses correspond to thermal strain. If during temperature changes of considered element, stresses do not exceed the yield stress $R_e(T)$, then after leveling the temperature to the ambient temperature, the state of stress vanishes and the considered element comes back to its primary. When stresses, induced by heterogeneous temperature field, exceed the yield stress $R_e(T)$ of element material, the plastic strains ε_{pl} are being formed inside it (they are equivalent to permanent strain ε_0). After self-cooling ($T = 0$) the element does not return to its primary shape. The state of residual stresses corresponds to the formed state of permanent strain.

The considered rod of rectangular section is subjected to mechanical loads characterized by internal forces $N = N(x)$ and $M_y = M_y(x)$ for the individual cross-sections. It is also subjected to symmetric action in relation to axis z in a slowly changing temperature field $T = T(x,y,z) = T(x,-y,z)$. This field is characterized by low temperature gradient in relation to a variable x. The state of stress of the rod is characterized by single dimensional state of stress $\sigma_x = \sigma_x(x,z,t)$ (Fig. 3), which fulfils integral conditions of equilibrium:

$$\begin{aligned}\int_{(A)} \sigma_x dA &= N(x) \\ \int_{(A)} \sigma_x z dA &= -M_y(x)\end{aligned} \tag{20}$$

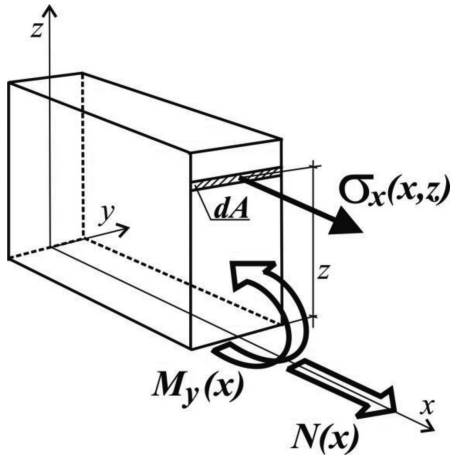

Fig. 3. Scheme of the rod subjected to loads

Area of the cross-section of the rod (in the solid state) changes due to weld penetration and solidification of the padding weld. Then, the position of the main axis of inertia is changing. Taking into account variability of the modulus of longitudinal elasticity in relation to coordinates of heterogeneous material of the rod, or Young's modulus dependent on temperature, and applying Hook's law $\sigma_x = E\varepsilon_x$, the solution is the following state of stress [24]:

$$\sigma = \frac{E}{A^E J_y^E - (S_y^E)^2}(J_y^E\left(N(x)+N^T\right)+S_y^E\left(M(x)-M_y^T\right)+ -\left(A^E\left(M(x)-M_y^T\right)+S_y^E\left(N(x)+N^T\right)\right)z)-E\varepsilon_0-\varepsilon^T E \tag{21}$$

where: $E = E(x, y, z, T)$– Young's modulus [MPa], $\sigma = \sigma(x, y, z, T)$,

$$A^E = A^E(x) = \int_{(A)} EdA, \quad S_y^E = S_y^E(x) = \int_{(A)} EzdA,$$

$$J_y^E = J_y^E(x) = \int_{(A)} Ez^2dA,$$

$$N^T = N^T(x) = \int_{(A)} \varepsilon^T EdA, \quad M_y^T = M_y^T(x) = \int_{(A)} \varepsilon^T EzdA.$$

Only in the case of thermal stress the equation (21) is different:

$$\sigma = \frac{E}{A^E J_y^E - (S_y^E)^2}(J_y^E N^T - S_y^E M_y^T + (A^E M_y^T - S_y^E N^T)z) - \varepsilon^T E) \tag{22}$$

4.2. The analysis of physical nonlinearity of rod's material

Stresses in elasto-plastic state are determined by iteration, using method of elastic solutions at the variable modulus of longitudinal elasticity conditioned by the stress-strain curve [25]. Function $\sigma = f(\varepsilon)$ applied in the iteration is obtained reproducing tension and compression curves. The border, below which unloading does not leave permanent strains is denoted by R_e. The first solution, which is the beginning of iteration for the determined external load and given permanent strain, is obtained on the basis of (23). If the obtained stress for the Young's modulus is in the plastic range $\left|\underset{(1)}{\sigma}\right| > R_e$ – (Fig. 4), then the change in modulus E must be done.

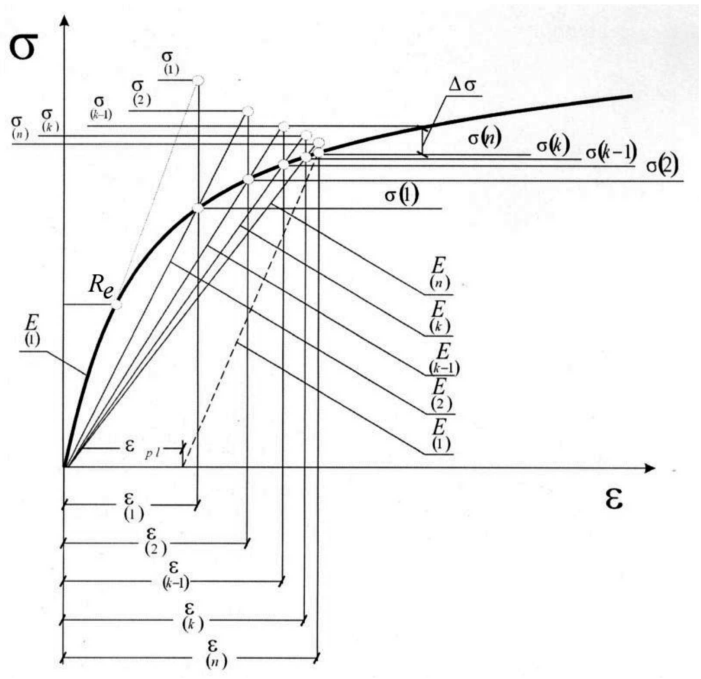

Fig. 4. Iteration of elasto-plastic states

The stress $\underset{(1)}{\sigma}$ corresponds to strain:

$$\underset{(1)}{\varepsilon} = \underset{(1)}{\sigma} / \underset{(1)}{E} \tag{23}$$

Stresses σ (1) are determined from the stress-strain curve for the strain $\underset{(1)}{\varepsilon}$, on the basis of which Young's modulus is defined:

$$\underset{(2)}{E} = \sigma(1) / \underset{(1)}{\varepsilon} \tag{24}$$

In every consecutive step k, the modulus E is iterated by modulus

$$\underset{(k)}{E} = \sigma(k-1) / \underset{(k-1)}{\varepsilon} \tag{25}$$

The stresses $\underset{(n)}{\sigma}$ (the n-th iteration step) are the final solution in the elasto-plastic range. They must fulfill the condition:

$$\left|\underset{(n)}{\sigma} - \sigma(n)\right| \leqslant \Delta\sigma \tag{26}$$

where $\Delta\sigma$ is the complex accuracy of solution. Then the plastic strain (permanent) is equal to:

$$\varepsilon_{pl} = \sigma(n) / \underset{(n)}{E} - \sigma(n) / \underset{(1)}{E} \tag{27}$$

5. The examples of computations and the results of experiment

Computations of temperature field and stress states, and measurement of residual stresses are carried out for the rectangular elements of dimensions ($h \times g \times l$) 60×8×600 mm made of S235 steel and surfaced by welding with GMA method. Computations and measurement of stresses are made for three values of welding current intensity (110, 124 and 151 A) at U = 65 V and v = 0.01 m/s.

5.1. Computations of temperature field, phase transformations and stresses

Temperature field is determined by the Rykalin's relationship [26] for the point model of a heat source:

$$T(z,t) = \frac{\eta_e UI}{vg\sqrt{4\pi c\rho t}} e^{-\left(\frac{z^2}{4at}+b_1 t\right)} \tag{28}$$

where: a – thermal diffusivity, $c\rho$ – thermal capacity, α_c – surface heat transfer coefficient, η_e – arc efficiency and

$$b_1 = \frac{2\alpha_c}{c\rho g} \tag{29}$$

The following properties of S235 steel: $c\rho = 5225376$ J/Km^3, $a = 8{\cdot}10^{-6}$ m^2/s, $\alpha_c = 31{,}4$ W/Km^2, $\eta_e = 0{,}65$, initial temperature $T_0 = 0$°C and solidus temperature 1493°C are assumed.

The detailed analysis of thermo-plastic states is carried out in the middle cross-section of the rod surfaced by welding at the current intensity 124 A.

Kinetics of phase transformations during heating is limited by the initial and final temperature of austenitic transformation, which are equal to $A_1 = 720$°C and $A_3 = 835$°C respectively. Temperature of solidus 1493°C determines fusion line. Maximum temperatures during surfacing in connection with temperatures A_1, A_3 and *solidus* determine characteristic heat affected zones (HAZ) for fusion, full and partial transformation as well as parent material. The progress of phase transformations during cooling is determined on a basis of TTT-welding diagram for S235 steel [27] presented in Fig. 5.

For examined steel in Eq. (10) is assumed $m = 1$ and $\mu = 0.012$ for $M_s = 410$°C, $M_f = 220$°C.

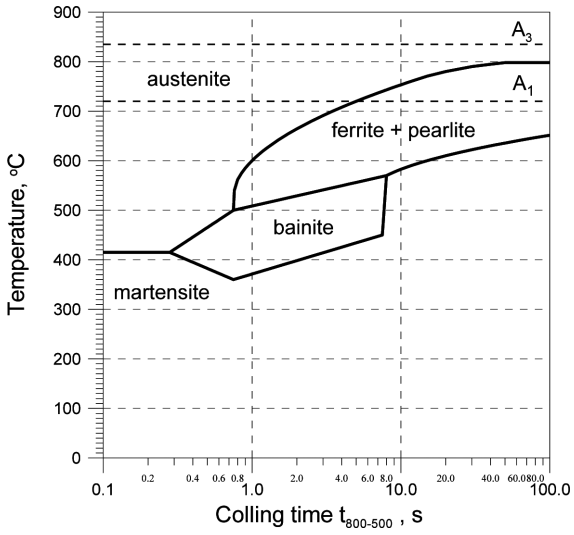

Fig. 5. TTT-welding diagram for S235 steel

In Figs. 6-8 are presented temperature changes and particular phase volume fractions at selected points of cross-section. At points $z = 0.03$ m (Fig. 6) from the fusion zone and points $z = 0.027$ m (Fig. 7) from full transformation zone, maximum temperatures exceed temperature A_3, full austenitic transformation occurs, while from overcooled austenite are created ca. 44% bainite, 39% ferrite and 17% pearlite. At points $z = 0.0261$ m (Fig. 8) from partial transformation zone during heating in austenite ca. 80% of parent structure transform. As a result of phase transformations of cooling, final phase fraction contains 36% bainite, 45% ferrite and 19% pearlite.

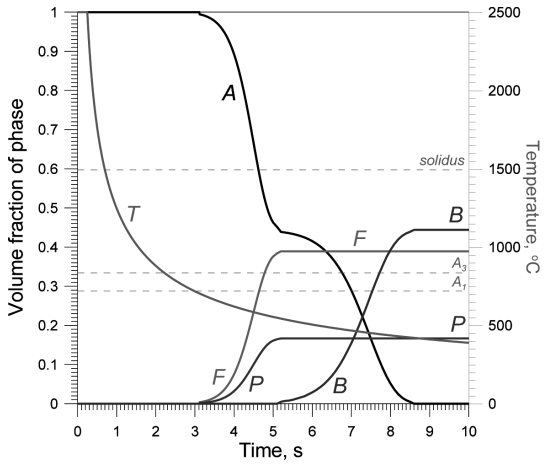

Fig. 6. Thermal cycle and particular phase volume fractions at points z = 0.03 m of the rod's cross section

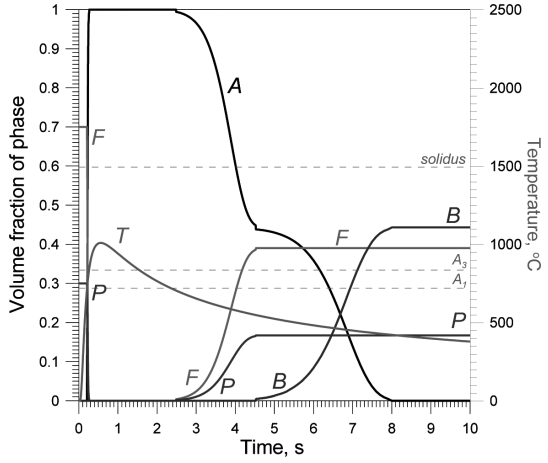

Fig. 7. Thermal cycle and particular phase volume fractions at points $z = 0.027$ m of the rod's cross section

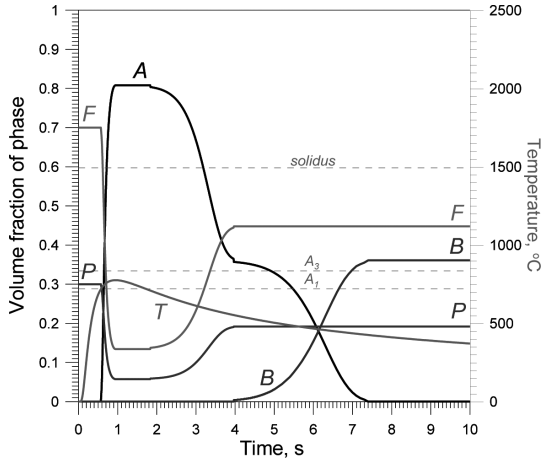

Fig. 8. Thermal cycle and particular phase volume fractions at points $z = 0.0261$ m of the rod's cross section

In computations of strains are assumed [28]:

– linear thermal expansion coefficients of ferrite and pearlite, $\alpha_F = \alpha_P = 1.534 \cdot 10^{-5}$ 1/K, bainite $\alpha_B = 1.171 \cdot 10^{-5}$ 1/K, austenite $\alpha_A = 2.178 \cdot 10^{-5}$ 1/K and martensite $\alpha_A = 2.178 \cdot 10^{-5}$ 1/K,
– structural strains of austenite into ferrite, pearlite and bainte as well as ferrite, pearlite, bainite and marteniste into austenite $\gamma_{AF=}\gamma_{AP} = \gamma_{FA} = \gamma_{PA} = 3.055 \cdot 10^{-3}$, $\gamma_{AB} = \gamma_{BA} = 4 \cdot 10^{-3}$, $\gamma_{AM} = 6.85 \cdot 10^{-3}$ respectively.

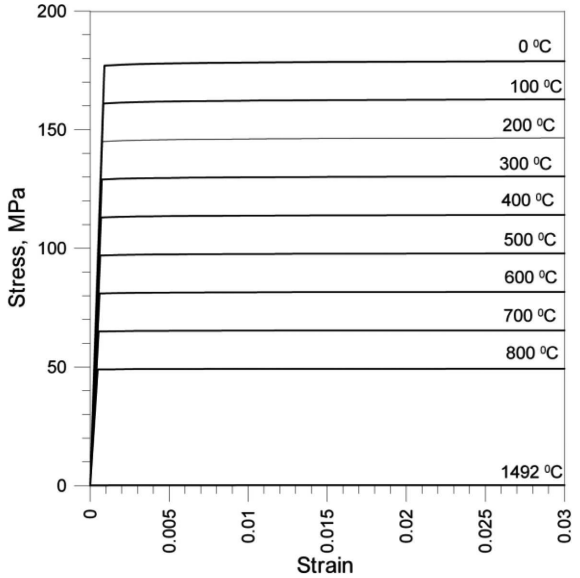

Fig. 9. The strain-stress curves of austenite in relation to temperature

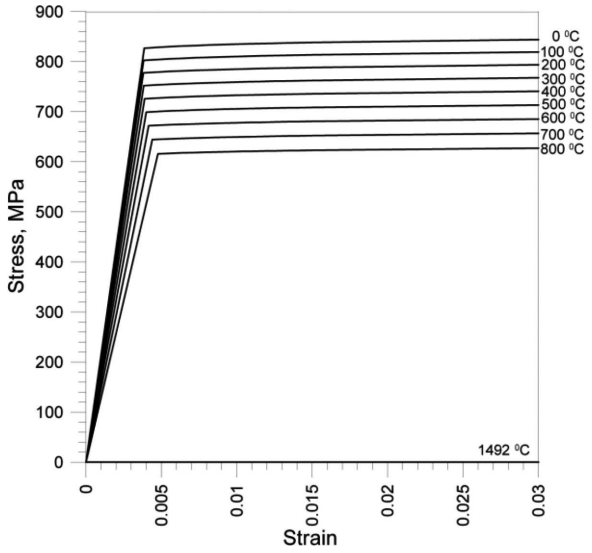

Fig. 10. The strain-stress curves of bainite in relation to temperature

Tensile curves of ferrite and pearlite are assumed on the basis of works [29, 30]. In case of austenite, bainite and martensite on the basis of data from works [31, 32] are determined tensile curves according to Swift law [33, 34]. The strain-stress curves for particulars structures in relation to temperature are presented in Fig. 11-15.

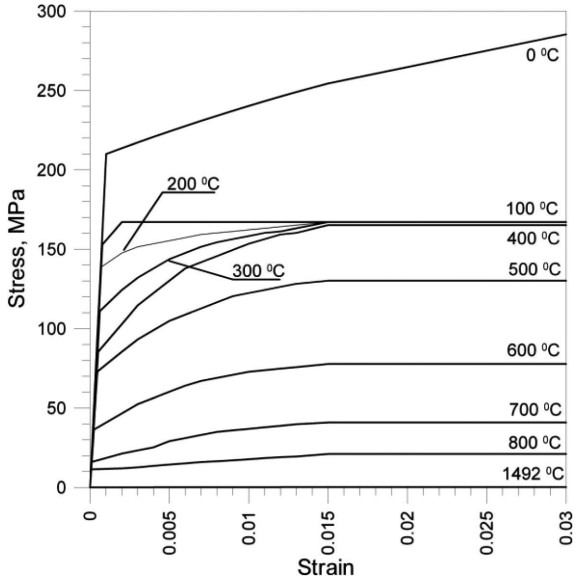

Fig. 11. The strain-stress curves of ferrite in relation to temperature

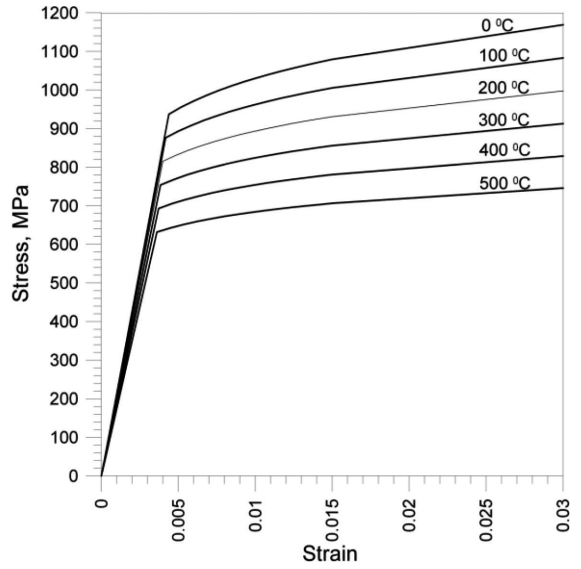

Fig. 12. The strain-stress curves of martensite in relation to temperature

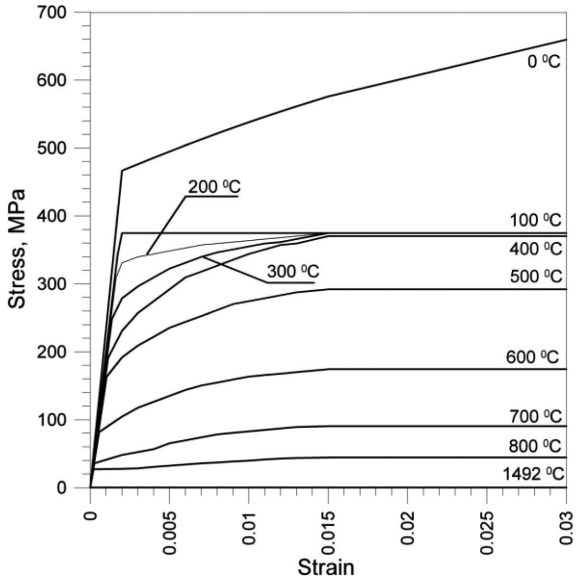

Fig. 13. The strain-stress curves of pearlite in relation to temperature

The detailed analysis of thermo-plastic states is carried out in the middle cross-section of the rod surfaced by welding at the current intensity 124 A, which is illustrated in Fig. 14 at selected points in time. In the initial phase, the zone of plastic weld penetration determined by temperature equal to 1493°C deepens due to propagation of heat supplied by electrode and reaches the depth of 0.002 m (Fig. 14a) 0.2 s after the passage of electrode. In this time compressive stresses are present in an adjacent region to the weld penetration, which leads to considerable plastic strains at the low yield point induced by temperature. Till 0.32 s – Fig. 14b, temperature drops in a liquid zone while solid zone heats up without changes in the boundary of weld penetration. By then, the material starts self-cooling process. Together with temperature decrease, the liquid zone solidifies and the consecutive layers of solidifying metal "stick" to the rod (Fig. 14c). The contraction of self-cooling material results in tensile stresses and plastic strains. Between solidus and 800°C a small increase in stresses accompanies considerable plastic strains due to the low yield point of material in this range of temperature. Solidification finishes at 0.7 s (Fig. 14d). A distinct drop in plastic strains chart at a height of cross-section between 0.0258 and 0.028 m (heat affected zone) is caused by transformation strains of overcooled austenite. Solidified layer after cooling contracts, while phase transformation strains cause compressive stresses in melted layer.

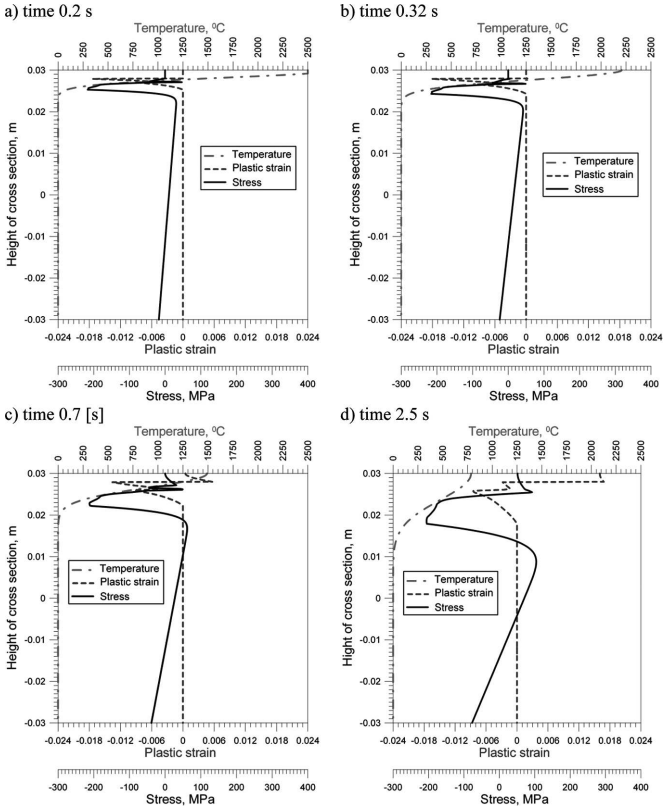

Fig. 14.(a-d) Temperatures, plastic strains and stresses in rod cross-wise section during surfacing

At the same time, negative plastic strains are reduced in the zone, which does not undergo plastic flow and tensile stresses zone is deepened (Fig. 14e).

Due to the maintenance of equilibrium of internal forces in the cross-section, an increase in region and in values of tensile stresses in the solidified layer and the zone of plastic strains created during heating, directly adherent to this layer, is accompanied by a reduction in tensile stresses in the middle part of the bar and by the decay of compressive stresses in the bottom part of the bar and then development of tensile stresses. In the final stage of solidification (Fig. 14f) changes in the stress field in the elastic range induced by thermal strains (shrinkage of the self-cooling material) can be observed. In heat affected zone values of tensile stresses on the surface of rod are low – 62 MPa (z = 0.03 m) and rise together with the depth to 380 MPa (z = 0.026 m). Then, in partial transformation zone, values slump to 238 MPa. The reason for this is the change of material structure. The yield stress of bainitic-ferritic-pearlitic structure is higher than of parent material, which does not undergo phase transformations.

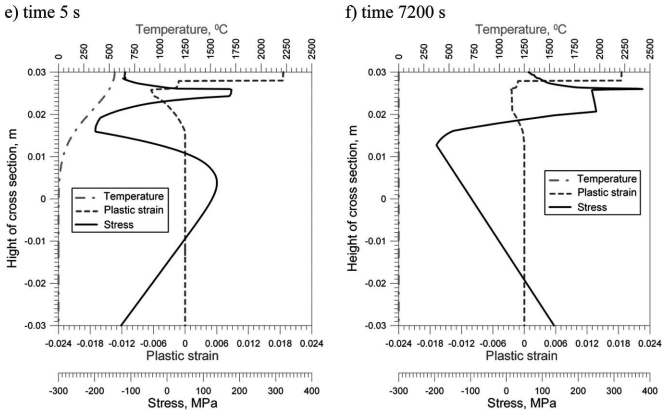

Fig. 14. (e-f) Temperatures, plastic strains and stresses in rod cross-wise section during surfacing

The history of these changes can be traced for selected points of cross-section. The point in the upper surface of rod (Fig. 15a), where heat source is applied, stays in the liquid phase to 0.7 s, and after this time the solidified material undergoes positive plastic strains and the tensile stresses are formed. Phase transformations of cooling cause a slight reduction of plastic strains and compressive stresses, which during further cooling transforms into tensile. At the point 2 mm (fusion line) from the surface – Fig. 15b, an intensive heating leads into plastic strains due to exceeding the yield point and compressive stresses which are caused by thermal extension of the material. Structural strains during heating cause a slight reduction of plastic strains and create tensile stresses, which then decrease as a result of further heating. Material reaches melting point after 0.2s. After solidification, positive plastic strains and tensile stresses occur. Phase transformations during cooling, first of austenite into ferrite and pearlite, and then of austenite into bainite, cause stresses to slump and the change of their sign. During further cooling tensile stresses occur. Their final reduction results from stress equilibrium in the cross-section. At a point in partial transformation zone (Fig. 15c) initial increase of tensile stresses is caused by stress equilibrium in the cross-section. Temperature increase causes creation of tensile stresses and negative plastic strains. Phase transformations cause sudden change of sign of stresses. This process stops when temperature reaches its maximum. During cooling tensile stresses slightly increase and plastic strains

are reduced. Phase transformations during cooling cause the sign of stress to change twice. Then further cooling causes the increase of tensile stresses. At a distance 10 mm from heated surface (Fig. 15d) initial increase of tensile stresses results from stress equilibrium in the cross-section, while as a result of thermal expansion of metal, and thereby intensive temperature increase, compressive stresses occur.

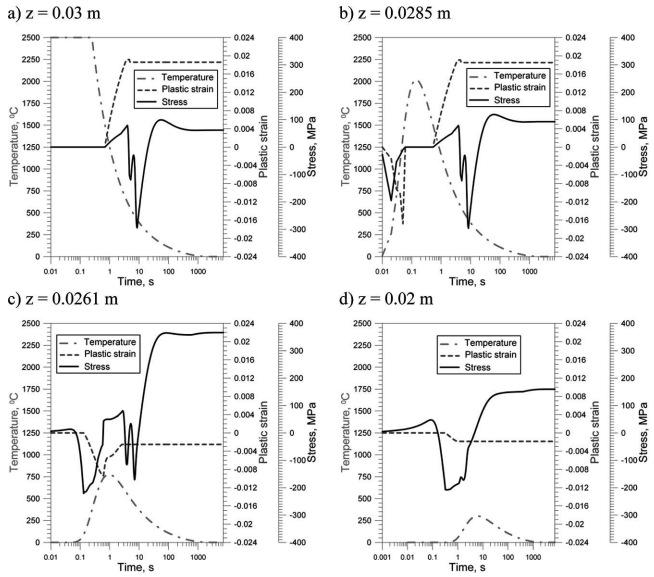

Fig. 15. Temperatures, plastic strains and stresses in selected points of rod crosswise section

After exceeding yield stress, negative plastic strains increase and compressive stresses are reduced. This lasts until temperature reaches its maximum. Then, during cooling compressive stresses decrease and tensile stresses occur. Slight drops on stresses chart are caused by structural strains of phases in the remaining part of cross-section, which are reflected in stress state of complete cross-section.

5.2. Experimental verification of the state of stress

Nine flat strength samples are made from the material used for cuboidal elements. For these samples the yield stress R_e =288 MPa is determined from the tested series. The Young's modulus is assumed at E = $2 \cdot 10^{-5}$ MPa for this material.

On side surface of surfaced elements were stuck extensometers at spots shown in Fig. 16 and Table 1. Then, parts of samples with stuck extensometers were cut out. A difference between the final and initial indications is the strain caused by "releasing" residual stresses, which are determined by an equation:

$$\sigma_i = -E\varepsilon_i \tag{30}$$

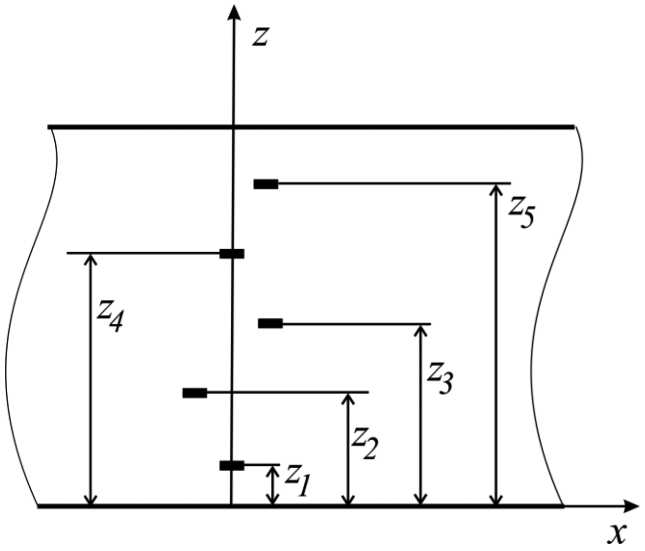

Fig. 16. The location of strain gauges

The stresses determined according to Eq. (28) are presented in Table 1. Residual stresses, calculated taking into account phase transformations and for homogenous material model [25], compared with experimental results are presented in Fig. 17. Diagrams of stresses are similar in shape for three calculated examples, but different as far as the depth of deposition of thermoplastic strains is concerned, due to the depth of penetration of heat source and the values of stresses in elastic range.

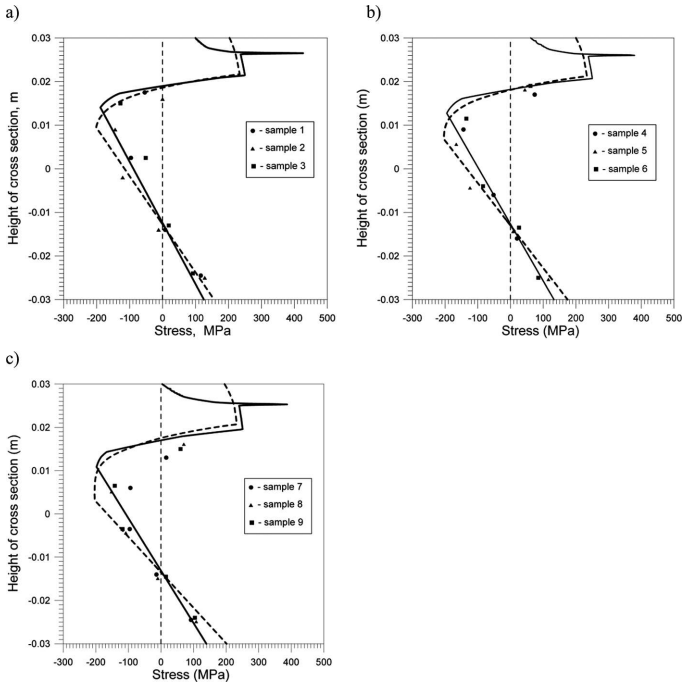

Fig. 17. Juxtaposition of the results of stress measurement with theoretical values for: a) series 1 (I = 110 A), b) series 2 (I = 124 A), c) series 3 (I = 151 A). Solid line marks theoretical distribution, which takes into account phase transformations, dashed line marks theoretical distribution, which does not take into account phase transformations (comp. Table 1)

TABLE 1

The experimentally obtained results of stresses for the tested cuboidal elements

Series No 1 I = 110 [A], d = 3.25 [mm]				Series No 2 I = 124 [A], d = 4 [mm]				Series No 3 I = 151 [A], d = 5 [mm]			
Number of sample	Number of point	z_i[mm]	σ_i[MPa]	Number of sample	Number of point	z_i[mm]	σ_i[MPa]	Number of sample	Number of point	z_i[mm]	σ_i[MPa]
1	1	5.5	116	4	1	5	-	7	1	5.5	92
1	2	16	8	4	2	14	20	7	2	16	-14
1	3	32.5	-96	4	3	24	-52	7	3	26.5	-96
1	4	47.5	-54	4	4	39	-144	7	4	36	-94
1	5	-	-	4	5	47	74	7	5	43	16
2	1	5	128	5	1	4.5	116	8	1	5	108
2	2	16	-12	5	2	15.5	8	8	2	15	-10
2	3	28	-121	5	3	25.5	-124	8	3	25.5	-108
2	4	39	-144	5	4	35.5	-166	8	4	35	-152
2	5	46	0	5	5	48	44	8	5	46	70
3	1	6	92	6	1	5	85	9	1	6	104
3	2	17	19	6	2	16.5	26	9	2	15.5	15
3	3	32.5	-51	6	3	26	-84	9	3	26.5	-118
3	4	45	-128	6	4	41.5	-135	9	4	36.5	-142
3	5	-	-	6	5	49	61	9	5	45	60

d – diameter of elektrode.

6. Conclusions

Presented model enables to assess the influence of temperature and phase transformations on strains and stresses (temporary and residual) in rod elements loaded thermally and mechanically. In particular it allows to:

– analyze thermal cycles in any given point of section, examine changes of volume fractions of phases and strains caused by temperature changes and phase transformations,
– analyze stress states and plastic strain field in rods during surfacing and residual stresses distribution after surfacing.

Distributions of measured residual stresses in surfaced flat confirm the correctness of assumptions and results of numerical simulations. Heterogeneity of material caused by phase transformations has influence mainly on values of tensile stresses in heat affected zone. The value of these stresses is determined not only by thermal load history, but also by the share of particular phase components and the value of yield stress. Residual stresses distribution in the area outside HAZ is affected mainly by the depth of plasticity. Maximal values of residual stresses in elastic zone are rising together with the depth of plasticity zone. When phase transformations are taken into account, calculated residual stresses in this area (outside HAZ) have slightly lower values than for homogenous material.

REFERENCES

[1] J.A. Goldak, A. Oddy, M. Gu, W. Ma, A. Mashaie, E. Hughes, Coupling heat transfer, microstructure evolution and thermal stress analysis in weld mechanics. In: Mechanical Effects of Welding, IUTAM Symposium Lulea, Sweden 1991, Springer Verlag Berlin Heidelberg 1991.

[2] Y. Ueda, J. Ronda, H. Murakawa, K. Ikeuchi, Thermo-mechanical-metallurgical model of welded steel. Part I: Evolution equations for internal material structures, Trans. JWRI **23**, 2, 148-167 (1994).

[3] J. Rońda, Y. Estrin, G.J. Oliver, Modelling of welding. A comparison of a thermo-mechano-metallurgical constitutive model with a thermo-viscoplastic material model, J. Mater. Proces. Technol. **60**, 629-636 (1996).

[4] J. Rońda, H. Murakawa, G Oliver, Y. Ueda, Thermo-mechanical-metallurgical model of welded steel. Part II: Finite element formulation and constitutive equations, Trans. JWRI **24**, 2, 92-113 (1995).

[5] L.E. Lindgren, Finite element modeling and simulation of welding. Part 1: Increased complexity, J. Thermal Stresses **24**, 141-192 (2001).

[6] L.E. Lindgren, Finite element modeling and simulation of welding. Part 2: Improved material modeling, J. Thermal Stresses **24**, 195-231 (2001).

[7] L.E. Lindgren, Finite element modeling and simulation of welding. Part 3: Efficiency and integration, J. Thermal Stresses **24**, 305-334 (2001).

[8] B. Chen, X.H. Peng, J.H. Fan, S.T. Sun, A viscous-elastoplastic constitutive equation incorporating phase

transformation with the application to the residual stress analysis for welding process, J. Mater. Proces. Technol. **205**, 316-321 (2008).

[9] D. D e n g, FEM prediction of welding residual stress and distortion in carbon steel considering phase transformation effects, Materials Design **30**, 359-366 (2009).

[10] A. B o k o t a, W. P i e k a r s k a, Numerical modeling of residual stresses in a dual laser beam welding, Metalurgija **49**, 2, 156-160 (2010).

[11] W. P i e k a r s k a, Numerical analysis of thermomechanical phenomena during laser welding process. The temperature fields, phase transformations and stresses. Monographies No 35, Technical University of Czestochowa (2007).

[12] N.O. O k e r b l o m, Welding strains and stresses, Mashgiz, Moscow-Leningrad 1948.

[13] D. R a d a j, Heat effects of welding. Temperature field, residual stress, distortion, Springer-Verlag, Berlin 1992.

[14] J. P i l a r c z y k, J. P i l a r c z y k, Arc welding and surfacing of metals, Slask sp. z o.o., Katowice 1996.

[15] E. T a s a k, Metallurgy of welding, JAK, Cracov 2008.

[16] J. R h o d e, A. J e p p s o n, Literature review of heat treatment simulations with respect to phase transformation, residual stresses and distortion, Scand. J. Metall. **29**, 47-62 (2000).

[17] W. P i e k a r s k a, M. K u b i a k, A. B o k o t a, Numerical simulation of thermal phenomena and phase transformations in laser-arc hybrid welded joint, Archives of Metallurgy and Materials **56**, 2, 409-421 (2011).

[18] M. A v r a m i, Kinetics of phase change. I. General theory, J. Chem. Physics **7**, 1103-1112 (1939).

[19] H.P. H o u g a r d y, Calculation of the transformation of steels on contionuous cooling, Metallurgy and Foundry **13**, 407-439 (1987).

[20] R. P a r k i t n y, J. W i n c z e k, Modelling of phase transformations during multipass surfacing, In:. Conf. Proc. XXXVI-II Sympozjon Modelling in Mechanics, Silesian University of Technology Gliwice, 219-224 (1999).

[21] D.P. K o i s t i n e n, R.E. M a r b u r g e r, A general equation prescribing the extent of the austenite-martensite transformation in pure iron-carbon alloys and plain carbon steels, Acta Mettall. **7**, 59-60 (1959).

[22] A. B o k o t a, T. D o m a ń s k i, Numerical analysis of thermo-mechanical phenomena of hardening process of elements made of carbon steel C80U, Archives of Metallurgy and Materials **52**, 277-288 (2007).

[23] T. D o m a ń s k i, A. B o k o t a, Numerical models of hardening phenomena of to ols steel base on the TTT and CCT diagrams, Archives of Metallurgy and Materials **56**, 325-344 (2011).

[24] J. W i n c z e k, A simplified method of predicting stresses in surfaced steel rods, J. Mater. Proces. Technol. **212**, 1080-1088 (2012).

[25] A. B o k o t a, R. P a r k i t n y, Modelling of thermal, structural and mechanical phenomena in hardening processes of steel elements. In: Informatics in Metal Technology, Silesian University of Technology, Gliwice (2003).

[26] M. M y s l i w i e c, Thermo-mechanical basis of welding, WN-T, Warszawa 1970.

[27] J. B r ó z d a, J. P i l a r c z y k, M. Z e m a n, Welding TTT diagrams of austenite transformations, Śląsk, Katowice 1983.

[28] J. W i n c z e k, A. K u l a w i k, Dilatometric and hardness analysis of C45 steel tempering with different heating-up rates, Metalurgija **51**, 1, 9-12 (2012).

[29] J. G a w ą d, D. S z e l i g a, A. B a t o r, V. P i d v y s o c k y y, M. P i e t r z y k, Interpretation of the tensile test results interpretation based on two criterion optimization, In: Proc. 14. Conf. KomPlasTech, Informatics in Metal Technology, ed. M. Pietrzyk et al., Akapit, Cracow, 27-34 (2004).

[30] P.M.M. V i l a R e a l, R. C a z e l i, L. S i m o e s d a S i l v a, A. S a n t i a g o, P. P i l o t o, The effect of residual stresses in the lateral-torsional buckling of steel I-beams at elevated temperature, J. Construct. Steel Research **60**, 783-793 (2004).

[31] M. M e l a n d e r, A Computional and Experimental Investigation of Induction and Laser Hardening, Linkoping Studies in Science and Technology, Dissertation No 124, Linkoping Univeristy (1985).

[32] J. L i a n, Z. J i a n g, J. L i u, Theoretical model for the tensile work hardening behaviour of dual-phase steel, Mater. Sci. Eng. **A147**, 55-65 (1991).

[33] Y.M. K i m, S.K. K i m, N.J. K i m, Correlation of yield ratio with materials constants of constitutive equation, Mater. Sci. Forum **475-479**, 289-292 (2005).

[34] S.K. K i m, Y.M. K i m, Y.J. L i m, N.J. K i m, Relationship between yield ratio and the material constants of the swift equation, Metals Materials Int. **12**, 2, 131-135 (2006).

Received: 20 November 2012.